

AUTHOR'S PERSONAL COPY



# RESEARCH MEMORANDUM

AN EXPERIMENTAL STUDY OF A METHOD FOR DESIGNING  
FUSELAGE SIDE AIR INLETS FOR HIGH PERFORMANCE  
AT TRANSONIC AND LOW SUPERSONIC SPEEDS

By Robert R. Howell and Charles D. Trescot, Jr.

Langley Aeronautical Laboratory  
Langley Field, Va.

CLASSIFIED DOCUMENT

This material contains information affecting the National Defense of the United States within the meaning of the espionage laws, Title 18, U.S.C., Secs. 793 and 794, the transmission or revelation of which in any manner to an unauthorized person is prohibited by law.

NATIONAL ADVISORY COMMITTEE  
FOR AERONAUTICS

WASHINGTON

January 17, 1956

CLASSIFICATION CHANGED TO UNCLASSIFIED  
AUTHORITY: NACA RESEARCH ABSTRACT NO. 129  
EXPIRATION DATE: JULY 17, 1958  
MIL

## NATIONAL ADVISORY COMMITTEE FOR AERONAUTICS

## RESEARCH MEMORANDUM

AN EXPERIMENTAL STUDY OF A METHOD FOR DESIGNING  
FUSELAGE SIDE AIR INLETS FOR HIGH PERFORMANCE  
AT TRANSONIC AND LOW SUPERSONIC SPEEDS


By Robert R. Howell and Charles D. Trescot, Jr.

## SUMMARY

A brief experimental investigation has been made of a method for designing fuselage side air inlets with high internal total-pressure recovery and zero spillage drag at a specified design inlet mass-flow ratio. With a scoop designed according to this concept, it was demonstrated experimentally that near-zero spillage drag can be attained at the design inlet mass-flow ratio through a Mach number range from 0.8 to 1.4. Achievement of an estimated total-pressure ratio of 0.99 at a Mach number of 1.4 was precluded only by a rapid thickening of the boundary layer ahead of the inlet. Although the fuselage boundary layer was fairly thick (the effective fineness ratio of the fuselage back to the inlet was 5.5), a mean total-pressure ratio of 0.94 was attained at the design inlet mass-flow ratio of 0.8 and a Mach number of 1.4. A maximum mean inlet total-pressure ratio of 0.96 was attained at a Mach number of 1.4 for a mass-flow ratio of 0.9.

## INTRODUCTION

Experimental work done on wing-root and fuselage side air inlets (refs. 1 and 2, for example) at Mach numbers in excess of 1.1 has indicated that the two major problems with such inlets at these speeds are the internal loss resulting from shocks and shock-boundary layer interaction ahead of the inlet and the drag due to the scoop. These losses in pressure recovery in this speed range penalize the performance of these fuselage side inlets as compared with nose inlets which do not have the boundary-layer problem. Some military aircraft which have, of necessity, resorted to the fuselage side type of inlet in order to have the fuselage nose space available for other purposes have generally taken some loss in performance by doing so, especially if the speed range of the airplane extended into the low supersonic regime.



An attempt has been made, therefore, to design a fuselage side inlet that would have high internal pressure recovery and low external drag at Mach numbers up to 1.4. The design is based on the theory of reference 3 and assumes that the flow field ahead of an infinite swept-back two-dimensional inlet may be treated similarly to the flow field ahead of an infinite sweptback wing.

Tests were made with the inlet mounted on the side of a body of revolution. Measurements included the total-pressure recovery at a station near the inlet and the external-drag increment due to the scoop. The ranges of Mach number and Reynolds number investigated were from 0.8 to 1.4 and from  $18.1 \times 10^6$  to  $27.8 \times 10^6$ , respectively. The tests were conducted in the Langley transonic blowdown tunnel at an angle of attack of  $0^\circ$ .

# SYMBOLS

A area, sq in.

$C_{DT}$  total drag coefficient,  $\frac{\text{Measured drag}}{q_o F}$

$C_{Db}$  base drag coefficient,  $-\frac{(p_b - p_o)}{q_o} \frac{A_b}{F}$

$C_{Di}$  internal drag coefficient due to momentum deficit,  
 $-\frac{m(V_x - V_o)}{q_o F} + \frac{(p_b - p_o)}{q_o} \frac{A_x}{F}$

$C_{D_{ext}}$  external drag coefficient,  $C_{DT} - C_{Db}$  for basic model and  
 $C_{DT} + (C_{Di} - C_{Db})$  for inlet model

$\Delta C_D$  incremental external drag coefficient due to scoop,  
 $C_{D_{ext, \text{inlet model}}} - C_{D_{ext, \text{basic model}}}$

$\frac{\bar{H}}{H_o}$  weighted total-pressure ratio,  $\frac{\int_A \frac{\rho_l V_l}{\rho_o V_o} \frac{H_l}{H_o} dA}{\int_A \frac{\rho_l V_l}{\rho_o V_o} dA}$

F frontal area of basic body, 3.14 sq in.

$\frac{m_i}{m_o}$  inlet mass-flow ratio,  $\frac{\rho_i V_i A_i}{\rho_o V_o A_i}$

P static pressure

V velocity

q dynamic pressure,  $\frac{\gamma}{2} \rho M^2$

$\rho$  mass density

M Mach number

Subscripts:

b base

i inlet, defined as normal to model axis at fuselage station 12.85

n normal to inlet leading edge

o free stream

l local

x exit

## MODELS, APPARATUS, AND TESTS

### Models

External design.- The inlet was designed on the theory that a two-dimensional sweptback inlet of infinite span would have a subsonic spillage drag characteristic and no losses in the entering flow if the leading edge is swept behind the Mach angle. This idea is analogous to Jones' swept wing theory (ref. 3). Under this concept, the resultant velocity at any point in the field about a two-dimensional inlet of infinite span which is swept back in the horizontal plane is the sum of two velocity components - one normal to the leading edge and one tangential to it. (See fig. 1.) The tangential component of velocity is constant throughout the flow field; the magnitude of the ratio of

tangential velocity to free-stream velocity depends entirely on the sweepback angle of the leading edge of the inlet. Any variation in the local resultant velocity and flow direction, therefore, is dependent only on the two-dimensional subsonic flow normal to the lip leading edge. Hence, the internal pressure recovery and inlet spillage drag of the sweptback two-dimensional inlet of infinite span should be associated only with the subsonic Mach number normal to the inlet leading edge although the free-stream velocity may be supersonic.

For the present case, the two-dimensional flow field (the field resulting from the flow normal to the inlet lip leading edge) was calculated in the following manner. The general flow characteristics were obtained by superimposing two basic flows. One is the flow out of a two-dimensional channel, the solution of which may be found in many text books, such as reference 4; the other is an opposing uniform potential flow. When the uniform flow is of greater strength than the flow out of the channel, addition of the two flows results in a net flow into the channel. The relative strengths of the two flows, therefore, determined the inlet velocity ratio  $V_{in}/V_n$  in the two-dimensional flow field (fig. 1(b)). For the present case, the two-dimensional inlet velocity ratio  $V_{in}/V_n$  was chosen such that when combined with the tangential velocity, the resultant total flow into the channel would correspond arbitrarily to  $\frac{m_1}{m_0} = 0.8$  at a Mach number of 1.4 assuming an isentropic compression.

After determination of the two-dimensional flow field of the channel for the specified inlet velocity ratio  $V_{in}/V_n$ , a modification had to be made to allow a finite lip thickness (fig. 1(b)). The finite lip thickness is required to allow construction of the model and to permit suction forces at the lip to offset spillage drag. For the present case, the two-dimensional channel wall was approximated by a thin inlet lip defined by elliptical ordinates, table I. The orthogonal flow net obtained by the superposition of the two basic two-dimensional flows was modified to correspond approximately to an experimentally determined pressure distribution for the new lip shape at the prescribed inlet velocity ratio. The modification was made by maintaining the general flow characteristics, adjusting the potential lines to correspond to the new lip pressure distribution and, then, rederiving the streamline shapes through the condition of orthogonality. The procedure used to obtain the two-dimensional flow field about the inlet as outlined, is not completely rigorous, but was chosen for expediency. A more precise but somewhat more laborious method of calculating the required two-dimensional flow field would be to follow a method as outlined in reference 5.

The local velocity ratio  $V_{ln}/V_n$  as calculated along streamlines in the two-dimensional field were adjusted for compressibility effects in

accordance with the Kármán-Tsien compressibility correction for a Mach number of 0.8. The Mach number of 0.8 was used for the correction inasmuch as it appeared to be about the highest Mach number for which the adjustment could be applied with a reasonable degree of accuracy.

Adjusted point values of velocity, as calculated from the two-dimensional flow field, were now added to the spanwise or tangential velocity component corresponding to the design sweepback angle of  $45^\circ$ , to obtain point values of the lateral slope of the streamlines passing inside and outside the inlet. These slopes were multiplied by increments of distance to obtain lateral displacements which were summed progressively from a point well ahead (station 8.00, fig. 2) of the inlet to a point behind the inlet lip leading edge corresponding to the maximum thickness station of the inlet lip. These calculated streamline shapes were then used to determine the shape of the solid boundary with which the sweptback inlet could be terminated on the upstream or inboard end without destroying the flow characteristics of the infinite inlet. The lateral shape of the streamlines approaching the inlet, theoretically approaches an isentropic compression surface for the particular design inlet mass-flow ratio. In many previously investigated scoop-type inlet designs the external compression has been accomplished with a wedge-type compression surface. (See for an example reference 6.) The downstream or outboard end of the inlet was terminated also, using calculated streamline shapes. The calculations were carried inside to the point where the flow became uniform in the duct (plane EE fig. 2). Downstream of this point, the longitudinal lines of the duct were faired to stream direction. In order to have sufficient outboard-end lip thickness, a  $5^\circ$  wedge angle was used between the inner and outer lip surfaces to define the external end-lip-surface slope (fig. 2). The wedge was arbitrarily faired to stream direction and cross-faired to the external side lips. Downstream of the line of inlet lip maximum thickness stations, all longitudinal elements of the scoop surface were made parallel to the axis of the body.

The now finite inlet was installed on a body of revolution without destroying the infinite inlet characteristics by shearing the streamlines relative to each other so that they conformed to the basic fuselage shape at a specified longitudinal location. This procedure is justified inasmuch as the streamline shape at any point in the field is independent of lateral location. For the present case, the calculated streamlines were rearranged to outline a two-inch-diameter circle at fuselage station 8.00 (fig. 2), which corresponds to the body shape on which the inlet was tested. The nose of the body used was made long (nose fineness ratio 4.0) to avoid any large induced velocity effects on the inlet design. The nose, which was a semiellipsoid of revolution, was combined with a cylinder to compose the basic body which had a total fineness ratio of 8.8. The effective fineness ratio of the body back to the inlet was about 5.5. The ratio of inlet area to basic body frontal area  $A_1/F$  was 0.20. A sketch

of the general arrangement of the scoop-body combination is presented in figure 2 and a photograph is shown as figure 3. Design ordinates are presented in table II.

Internal duct design.- The internal duct was of constant cross-sectional area back to station 12.85, the forward measuring station. Rearward from this station to station 14.65, the flow was diffused through an area ratio of about 1.3 to 1.0 in a two-dimensional diffuser having an effective  $8.5^\circ$  two-dimensional diffuser angle. Between station 14.65 and station 17.65, the duct area was gradually contracted to the area at the exit station. The exit area was varied by adjusting the lower surface of the diffuser which was pivoted at the end of the subsonic diffuser (station 14.65). The lower surface was sealed against pressure leaks after each area setting and an inspection was made after each test point to insure correct measurements. The longitudinal cross-sectional shape of the duct is shown in figure 2.

#### Instrumentation

The pressure instrumentation of the model included a forward measuring rake consisting of 17 total-pressure and 2 static-pressure tubes, an exit measuring rake consisting of a total of 16 total-pressure and 2 static-pressure tubes (fig. 4), and static-pressure probes in the model base and in the cavity between the effuser flap and basic model surface. The number of total-pressure tubes actually used for measuring in the exit varied from 16 to 11 depending on the exit flap setting. (See fig. 4.)

Drag force measurements were obtained by use of an internal strain-gage balance.

#### Measurements

The total and static pressures measured at the forward measuring station, were used to obtain point values of total-pressure ratio and the corresponding values of local mass-flow ratio. These point values were numerically integrated over the local area to obtain the mean weighted values of total-pressure ratio  $\bar{H}/H_0$  and corresponding inlet mass-flow ratio,  $m_1/m_0$ .

For the force tests, the measured pressures at the exit measuring station were similarly used, that is, point values of local mass-flow ratio and internal drag were computed and integrated. The inlet rake was removed for these tests and as a result it was possible to obtain drag data at inlet mass-flow ratios up to 1.0. The static pressure was

measured independently in the two separate base areas indicated in figure 2 and the base drag was obtained through the use of these pressures and their respective areas.

Force measurements were made on the basic body of revolution and on the body with the scoop installed. For some of the tests, oil flow studies were made to determine the direction of boundary-layer flow ahead of the inlet.

### Tests

The tests were conducted in the Langley transonic blowdown tunnel through a range of Mach number from 0.8 to 1.4. The corresponding Reynolds number based on the model length varied between  $18.1 \times 10^6$  and  $27.8 \times 10^6$ .

The model was sting-mounted in the tunnel at an angle of attack of  $0^\circ$ . The angle of attack was set with a sensitive inclinometer and was unchanged during the investigation.

On the basis of schlieren photographs and previous experience, it appears that shock reflected disturbances possibly prevent the drag increment due to the scoop installation from being valid in the Mach number range between about  $M_0 = 1.02$  and about  $M_0 = 1.18$ . No force data are presented for this particular Mach number range. For a small range of Mach number greater than 1.18, the reflected bow wave intersected only the parallel elements of the afterbody thereby causing no deviation in pressure drag; the scoop pressure-drag increments obtained at Mach numbers greater than 1.18, therefore, are believed to be correct.

Below is a table of the more pertinent parameters and the estimated maximum experimental error for each:

$M_0$ . . . . .	$\pm 0.01$
$\bar{H}/H_0$ . . . . .	$\pm 0.01$
$m_1/m_0$ . . . . .	$\pm 0.02$
$C_{D_{ext}}$ . . . . .	$\pm 0.015$

Generally, it is believed that the actual error is considerably less than these estimated maximums.



## RESULTS AND DISCUSSION

## Pressure Recovery

Point values of total-pressure ratio  $H_t/H_o$  as measured at the forward measuring station for a  $\frac{m_1}{m_o} \approx 0.8$  are presented in figure 5 for the various test Mach numbers. The local total-pressure ratios in the outboard portion of the inlet were very high, varying between 1.0 and 0.98 in the Mach number range between 0.81 and 1.4.

It should be noted that at a Mach number of 1.4, the theoretical inlet total-pressure ratio would not be exactly 1.0. The inability to attain the ideal or isentropic results is due to the fact that at this Mach number the tangential velocity approaches the speed of sound and the addition of the normal velocity component causes the resultant Mach number to approach 1.15. As a result, a compression wave ahead of the outboard end of the inlet lip decelerates the flow and causes a small loss in total pressure. It is estimated that for this case the inlet total-pressure ratio would be about 0.99.

Schlieren photographs of the flow entering the inlet (fig. 6) indicate that some form of compression wave existed in front of the scoop at all supersonic Mach numbers. No normal shocks were observed, however, and there is some evidence of wavelets either at or following the inclined shock wave. An indication that the actual compression approached the theoretical is the presence of point values of total-pressure ratio of 0.99 in the outboard end of the inlet (fig. 5). At supersonic Mach numbers, losses in recovery apparently due to the entrainment of some of the fuselage boundary layer are observed in the inboard portion of the inlet. It is indicated by the photographs of oil flow patterns presented in figure 7 that considerable bypassing of the fuselage boundary layer around the inlet resulted from the transverse pressure gradients afforded by the design. It appears, then, that the amount of boundary layer that entered the inlet is probably only a small part of the boundary layer that would wash the surface if the inlet were not there. Hence, the increase in losses with Mach number in the lower portion of the inlet, probably results largely from the adverse effect of the increasing pressure rise with Mach number on the boundary layer that does enter the inlet at any specific inlet mass-flow ratio. The improvement in mean total-pressure ratio obtained by increasing inlet mass-flow ratio from 0.8 to 0.9 at  $M_o = 1.40$ , (fig. 8) appears to result primarily from the corresponding improvement in the adverse pressure gradient between the sweptback inlet lips resulting in less loss due to the entering boundary layer (see fig. 5). The use of continuous boundary-layer suction through a porous compression surface between the

inlet lips would probably reduce the total-pressure losses due to the entering boundary layer.

The mean values of total-pressure ratio as measured at the inlet measuring station are presented in figure 9 as a function of Mach number for two inlet mass-flow ratios. At an inlet mass-flow ratio of 0.9, the total-pressure ratio ranges from  $\frac{\bar{H}}{H_0} = 0.99$  at  $M_0 = 0.80$  to  $\frac{\bar{H}}{H_0} = 0.96$  at  $M_0 = 1.4$ . At a mass-flow ratio of 0.8, the ratio drops to  $\frac{\bar{H}}{H_0} = 0.94$  at  $M_0 = 1.4$ . These total-pressure ratios are considered to be quite high for a scoop-type air inlet placed 5.5 diameters back from the nose. (See, for example, reference 6.)

Although it was not the purpose of the present investigation to determine internal diffuser losses, some additional pressure recovery information obtained at the exit station after a subsonic diffusion indicates the ability of the design concept investigated to provide high pressure ratios at not only the inlet measuring station, but also at an engine compressor entrance. Presented in figure 10 are the mean exit total-pressure ratios as a function of Mach number for two exit flap settings. These measurements were made during the drag tests when the inlet rake was removed. Also presented for comparison are the mean total-pressure ratios as measured at the same inlet mass-flow ratios for an open nose inlet in free flight (ref. 7). In this case, the total-pressure ratios were measured at the end of a conical diffuser having about a  $3^\circ$  included angle and an area ratio of 2.3 to 1.0. As can be seen, the mean exit total-pressure ratio for the present scoop inlet design was only about 2 to 3 percent lower than that measured for the nose inlet configuration at a Mach number of 1.4.

#### Drag Due to the Scoop

The external drag increment incurred by installing a scoop on a body or airframe is generally considered to include: (1) a pre-entry and an inlet lip pressure force associated with reducing the momentum of the entering fluid to satisfy the inlet operating condition at a reduced inlet flow rate, (2) the scoop afterbody or form pressure force associated with the possible fairing of the scoop into the airframe and (3) the viscous force increment resulting from changes in the total wetted area due to installation of the scoop.

For the present case, the afterbody or form pressure force was not permitted inasmuch as parallel elements were used to define the after portion of the scoop and fuselage. Hence, the presented increments of

external drag due to the scoop include only the pre-entry and lip pressure forces and, of course, the added viscous forces due to the increase in total wetted area. These increments (fig. 11) are the differences between the external drags of the scoop-body combination and the drags of the body alone and are presented as a function of Mach number for various inlet flow rates.

It should be noted that of the total 0.03 increment in drag coefficient due to the scoop indicated in the subsonic speed range, only about 0.02 can be directly attributed to the increase in wetted area due to installing the scoop on the basic body. The remaining inconsistency of 0.01 in incremental drag coefficient is within the estimated error presented in the section entitled "Tests."

At the design inlet mass-flow ratio of 0.8, near zero pressure drag was obtained through the test Mach number range. This result is in accordance with the theory used for the design of the inlet, that is, the spillage at the inlet occurs primarily as two-dimensional subsonic flow normal to the sweptback inlet lips as a result of the detailed shaping of the fuselage surface. For the  $m_1/m_0 = 0.8$  case, then, the scoop inlet was added to the body at a drag cost equal to about the viscous drag increase.

At the inlet mass-flow ratios other than the design value ( $m_1/m_0 = 0.7$  and  $1.0$ ), the variation of drag-coefficient increment with Mach number was small and generally was within the possible error of the tests. Hence, although the indicated variation in drag-coefficient increment with Mach number at the off-design conditions was probably as would be expected, the only justifiable conclusion that may be drawn is that only a small pressure-drag variation with Mach number resulted from installing the scoop inlet and operating it at inlet mass-flow ratios as low as 0.7. At  $m_1/m_0 = 0.7$ , the pressure-drag increase due to the scoop was indicated to be only 0.02 at  $M_0 = 1.4$ . Assuming that the ratio of fuselage frontal area to wing area is 0.06 (which is about average for high-speed designs), the corresponding pressure-drag increment based on the wing area is only 0.0012.

It should be remembered that the presented drag-coefficient increments are due only to the inlet design and do not include any form drag associated with the possible fairing of the scoop back into the fuselage. It should be further noted that these latter pressure drags (those due to the afterbody fairing) may vary considerably between configurations having different types of engine-inlet installations. For the case of engines buried in the wing root, very little fairing would be needed. In the light of the development of the area-rule principle (ref. 8), it would be expected that the final drag increment attained from a scoop-inlet installation would depend largely on how well the designer

incorporated the scoop into the overall area development of the particular airframe.

#### CONCLUDING REMARKS

A method for designing fuselage side air inlets with high internal total-pressure recovery and zero spillage drag at a specified design Mach number and inlet mass-flow ratio has been presented.

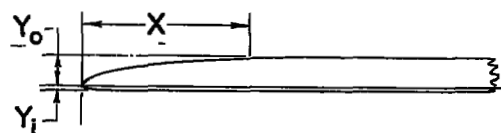
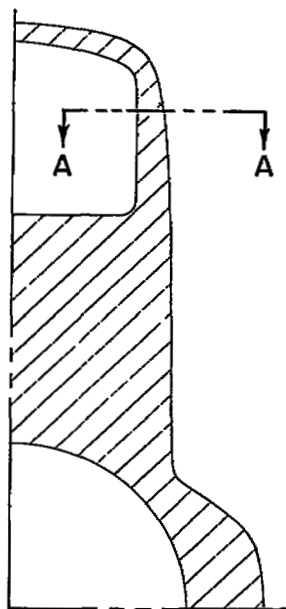
It was shown experimentally that an inlet designed according to this concept would have near-zero spillage drag at the design inlet mass-flow ratio of 0.8 through a Mach number range from 0.8 to 1.4. It was further indicated that the theoretical estimated total-pressure recovery of 99 percent was precluded only by a thickening of the boundary layer ahead of the inlet. Although the fuselage boundary layer was fairly thick (the effective fineness ratio of the fuselage length back to the inlet was 5.5), a mean inlet total-pressure ratio of 0.94 was attained at the design inlet mass-flow ratio of 0.8 and a Mach number of 1.4. A maximum mean inlet total-pressure ratio of 0.96 was attained at a Mach number of 1.4 for a mass-flow ratio of 0.9.

Langley Aeronautical Laboratory,  
National Advisory Committee for Aeronautics,  
Langley Field, Va., July 14, 1955.

## REFERENCES

1. Howell, Robert R., and Trescot, Charles D., Jr.: Investigation at Transonic Speeds of Aerodynamic Characteristics of a Semielliptical Air Inlet in the Root of a  $45^{\circ}$  Sweptback Wing. NACA RM L53J22a, 1953.
2. Carter, Howard S., and Merlet, Charles F.: Flight Determination of the Pressure Recovery and Drag Characteristics of a Twin Side-Inlet Model at Transonic Speeds. NACA RM L53EO5, 1953.
3. Jones, Robert T.: Wing Plan Forms for High-Speed Flight. NACA Rep. 863, 1947. (Supersedes NACA TN 1033.)
4. Streeter, Victor L.: Fluid Dynamics. McGraw-Hill Book Co., Inc., 1948.
5. Perl, W., and Moses, H. E.: Velocity Distributions on Two-Dimensional Wing-Duct Inlets by Conformal Mapping. NACA Rep. 893, 1948.
6. Davis, Wallace F., and Edwards, Sherman S.: Experimental Investigation at Supersonic Speeds of Twin-Scoop Duct Inlets of Equal Area. III - Inlet Enclosing 37.2 Percent of the Maximum Circumference of the Forebody. NACA RM A8EO4, 1948.
7. Sears, Richard I., and Merlet, C. F.: Flight Determination of Drag and Pressure Recovery of a Nose Inlet of Parabolic Profile at Mach Numbers from 0.8 to 1.7. NACA RM L51EO2, 1951.
8. Whitcomb, Richard T.: A Study of Zero-Lift Drag-Rise Characteristics of Wing-Body Combinations Near the Speed of Sound. NACA RM L52HO8, 1952.

TABLE I .-DESIGN COORDINATES FOR INLET SIDE LIP SHAPE  
(All dimensions are in inches)

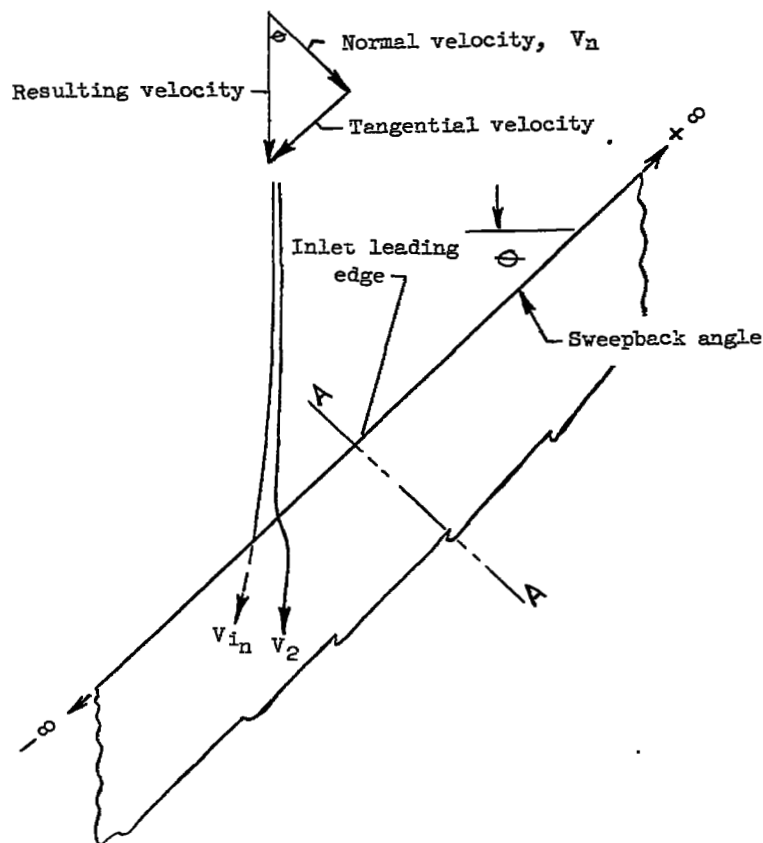


Section A-A

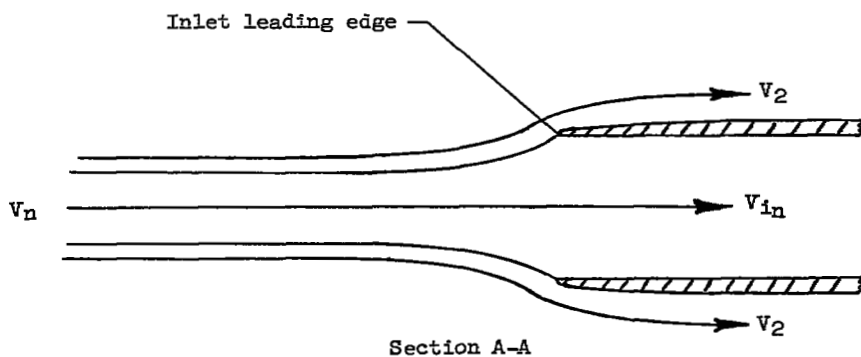
Inlet side lip

Coordinates for inlet side lip		
X	$Y_o$	$Y_i$
0.000	0.000	0.000
.010	.018	.007
.020	.025	.010
.030	.030	.012
.040	.035	.014
.050	.039	.015
.075	.047	.015
.100	.054	.015
.200	.075	.015
.300	.089	.015
.400	.100	.015
.500	.108	.015
.600	.114	.015
.700	.119	.015
.800	.122	.015
.900	.124	.015
1.000	.125	.015





(a) Plan view sketch showing lateral streamline paths into and over the inlet.



(b) Sketch of section taken normal to inlet leading edge showing streamline paths in vertical plane.

Figure 1.- Sketches showing streamline paths into and over a two-dimensional sweptback inlet of infinite span.



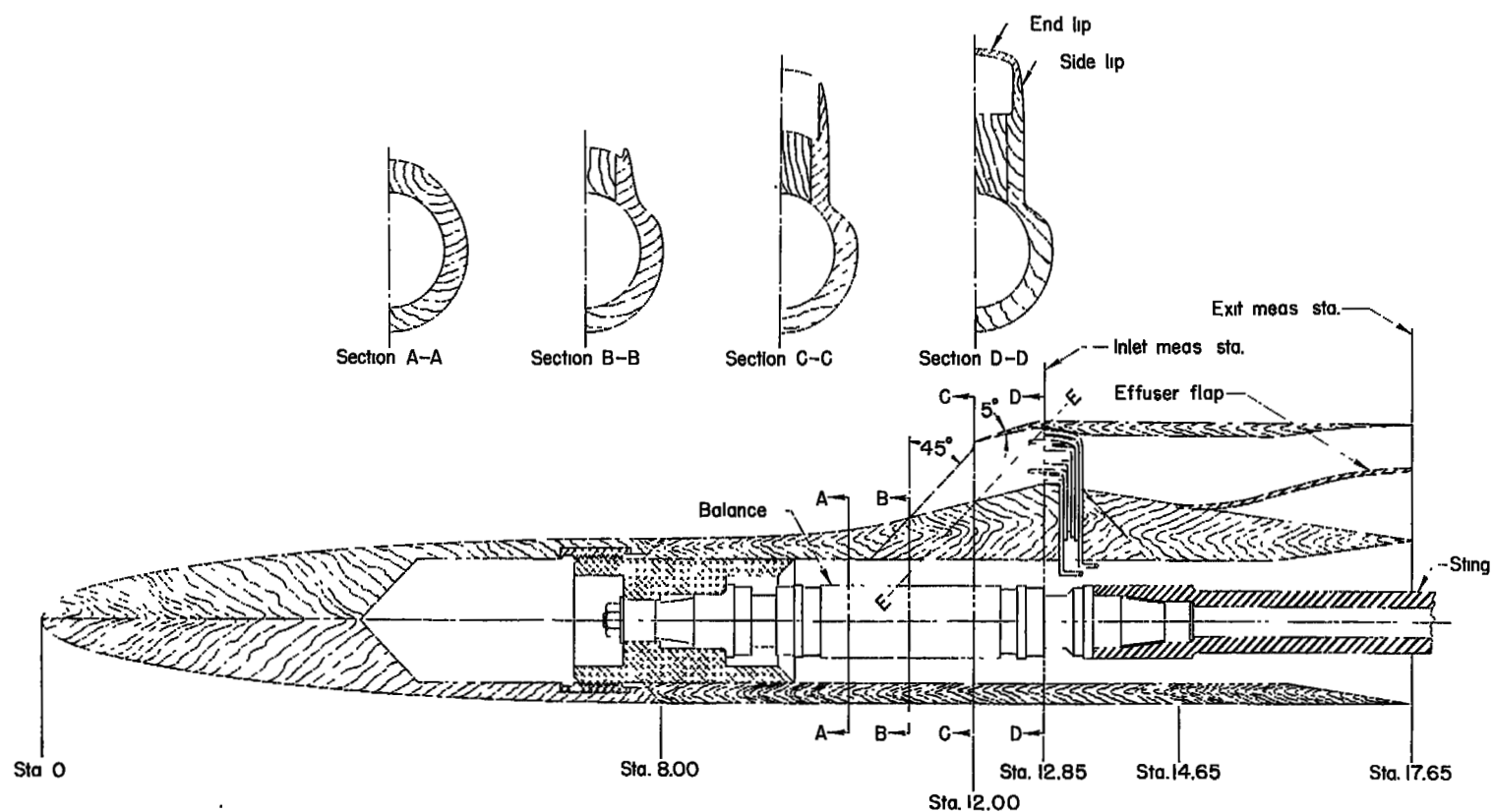


Figure 2.- Diagrammatic sketch showing details of force and pressure measurements and internal flow arrangement.

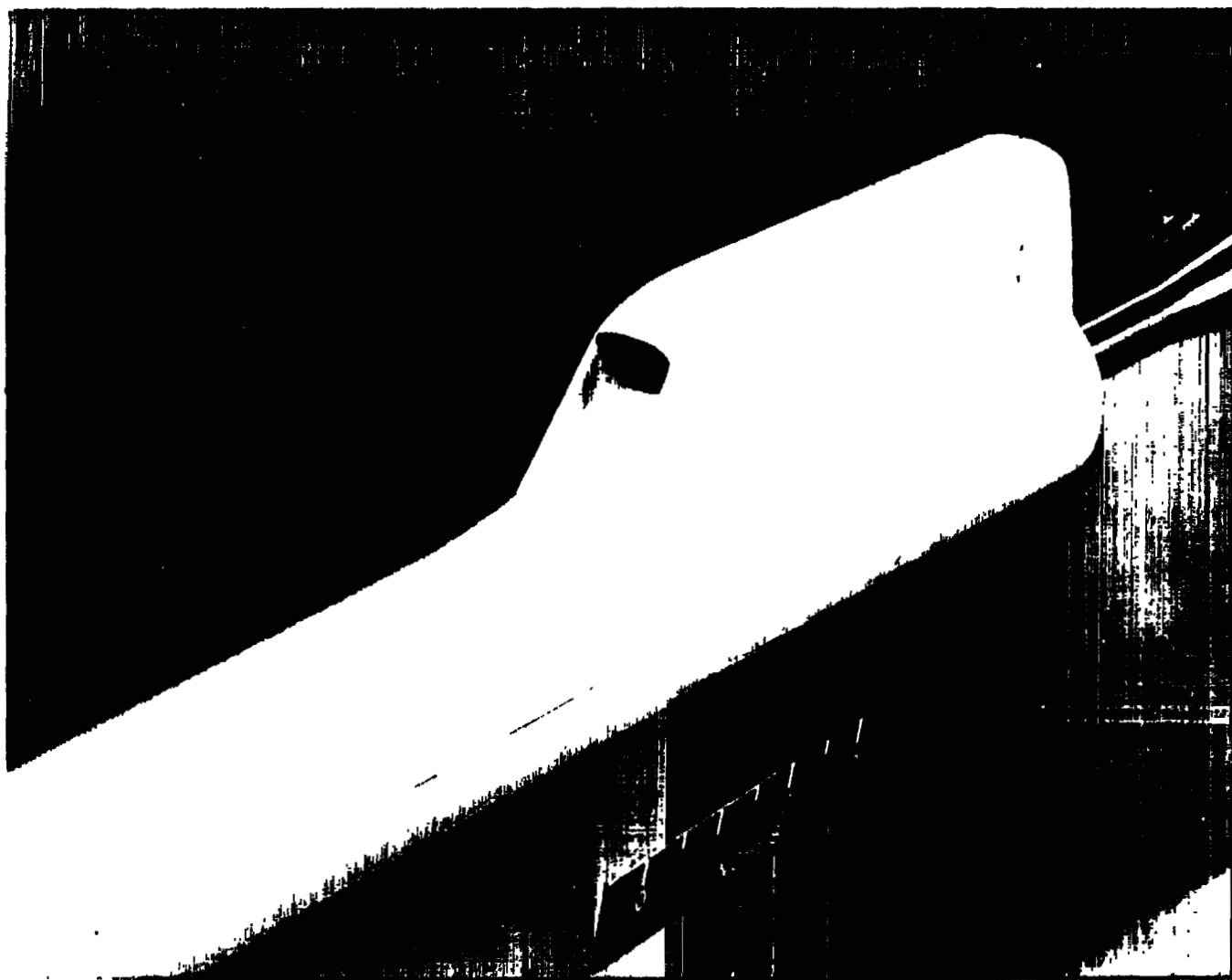
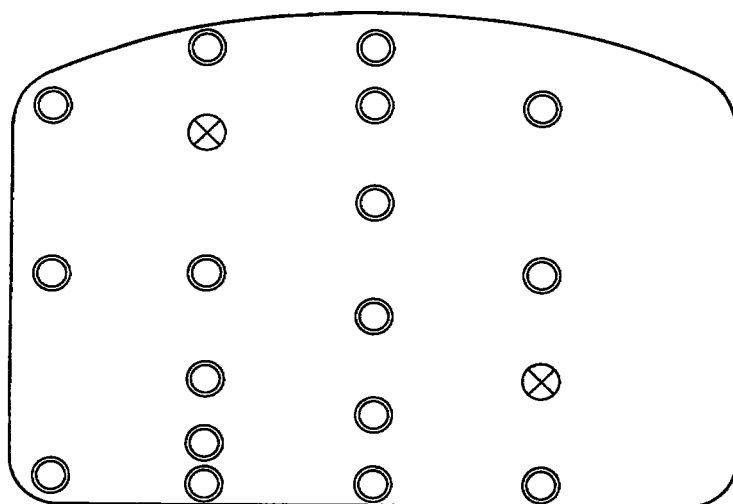
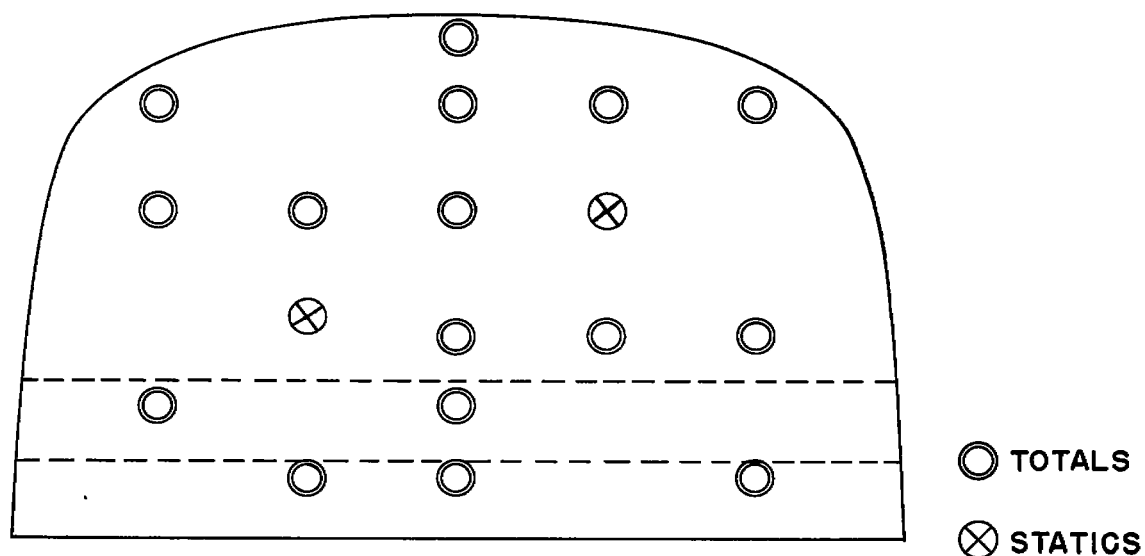


Figure 3.- Three-quarter view photograph of scoop.

L-85116



TUBE DISTRIBUTION AT THE INLET  
MEASURING STATION



TUBE DISTRIBUTION AT THE EXIT  
MEASURING STATION

Figure 4.- Total- and static-pressure tube distributions at the inlet  
and exit measuring stations.

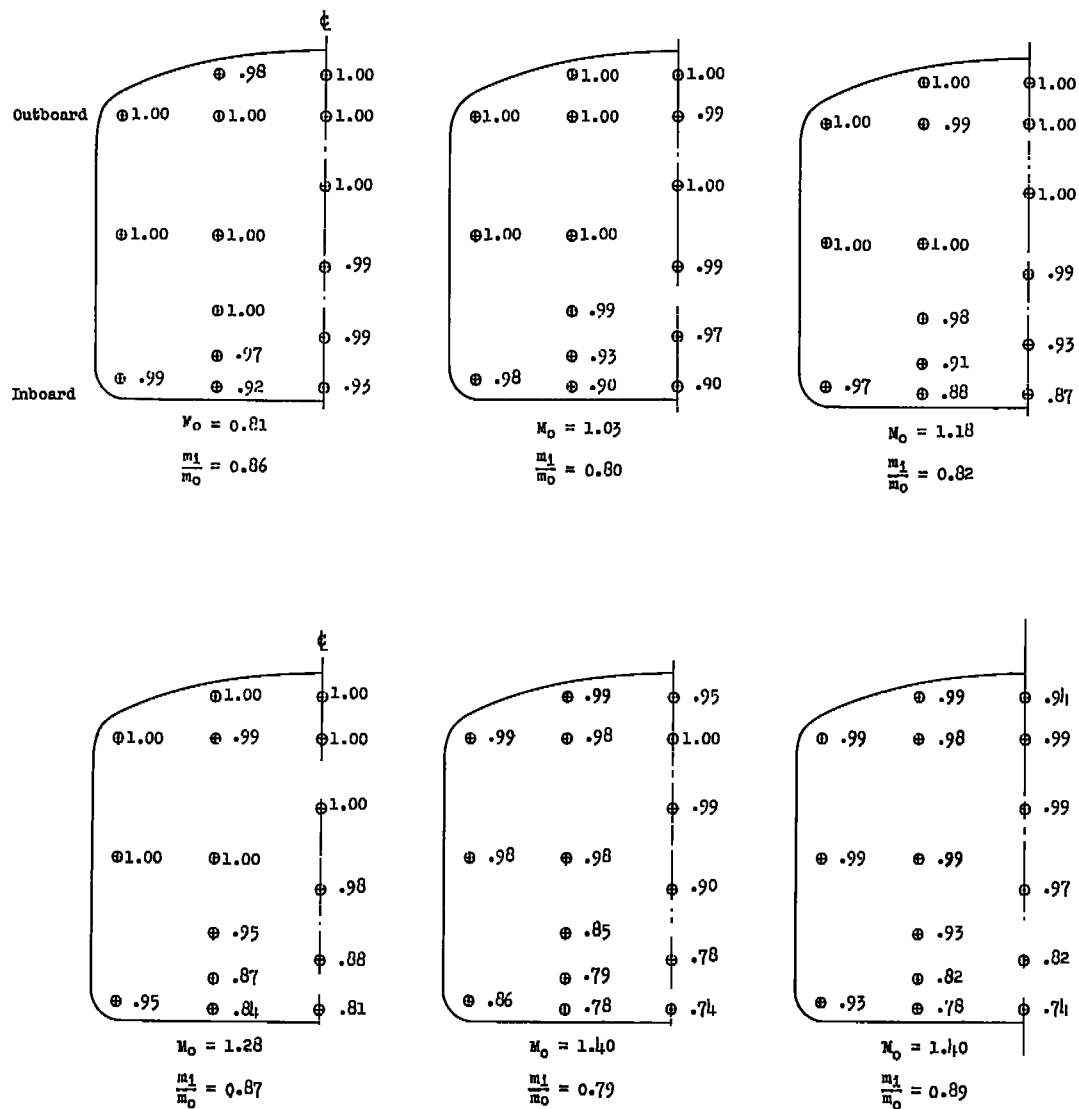
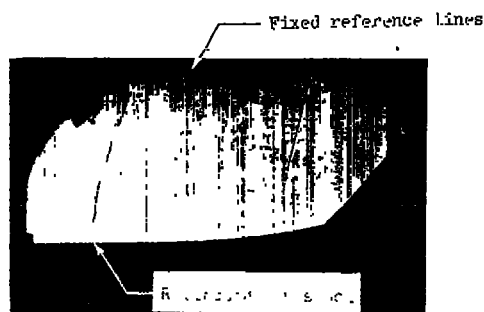
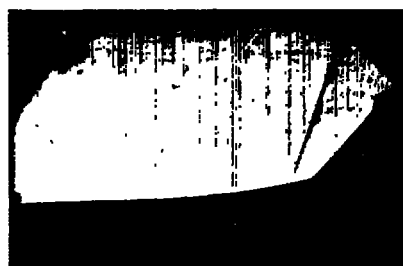


Figure 5.- Point values of total-pressure ratio for various Mach numbers as measured at the forward measuring station.



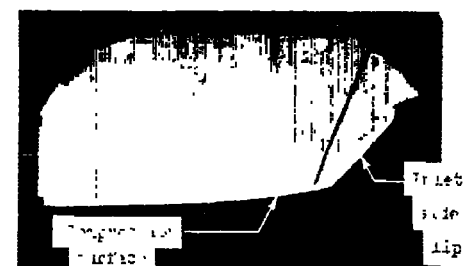
$$M_0 = 1.13$$

$$\frac{m_1}{m_0} = 0.86$$



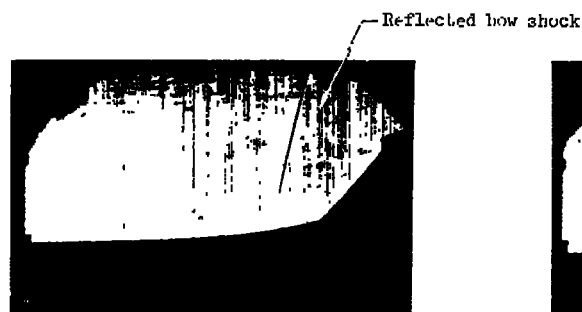
$$M_0 = 1.24$$

$$\frac{m_1}{m_0} = 0.89$$



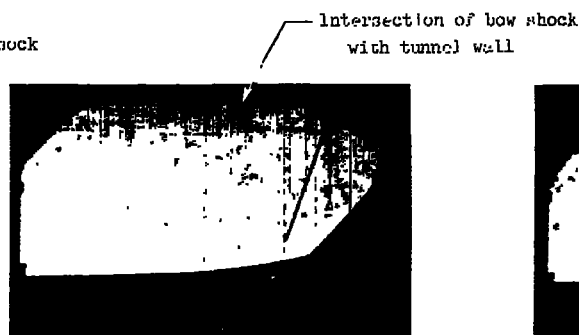
$$M_0 = 1.40$$

$$\frac{m_1}{m_0} = 0.90$$



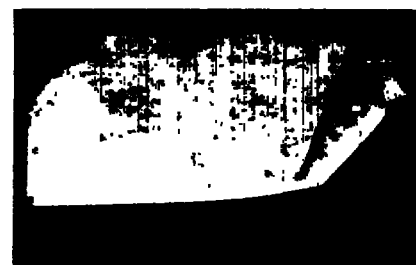
$$M_0 = 1.16$$

$$\frac{m_1}{m_0} = 0.76$$



$$M_0 = 1.34$$

$$\frac{m_1}{m_0} = 0.73$$



$$M_0 = 1.40$$

$$\frac{m_1}{m_0} = 0.70$$

L-89370

Figure 6.- Schlieren photographs of flow ahead of the scoop for various

Mach numbers.  $\frac{m_1}{m_0} \approx 0.9$  and  $\frac{m_1}{m_0} \approx 0.7$ .



$$M_O = 1.12$$

$$\frac{m_1}{m_0} = 0.92$$



$$M_O = 1.27$$

$$\frac{m_1}{m_0} = 0.93$$



$$M_O = 1.39$$

$$\frac{m_1}{m_0} = 0.93$$



$$M_O = 1.18$$

$$\frac{m_1}{m_0} = 0.66$$



$$M_O = 1.27$$

$$\frac{m_1}{m_0} = 0.66$$



$$M_O = 1.40$$

$$\frac{m_1}{m_0} = 0.70$$

Figure 7.- Oil-flow patterns described by flow ahead of and into the scoop at various Mach numbers.  $\frac{m_1}{m_0} \approx 0.9$  and  $\frac{m_1}{m_0} \approx 0.7$ .

L-89371

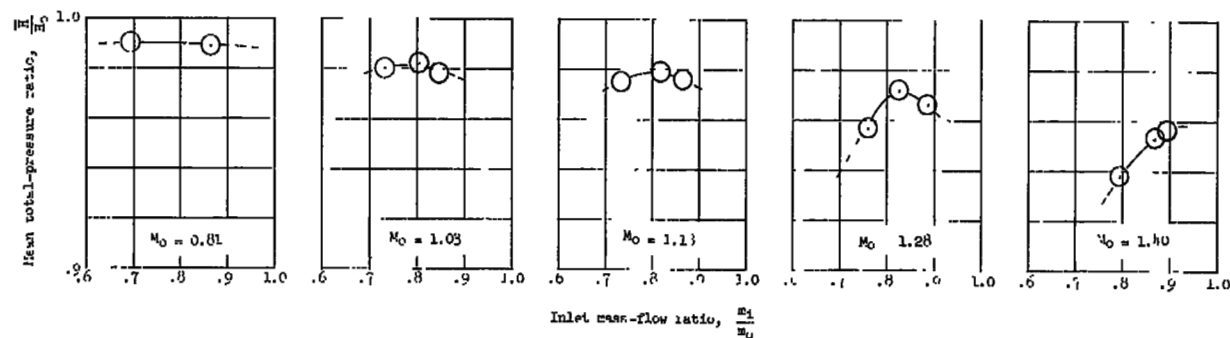


Figure 8.- Variation of mean total-pressure ratio with inlet mass-flow ratio at various test Mach numbers.

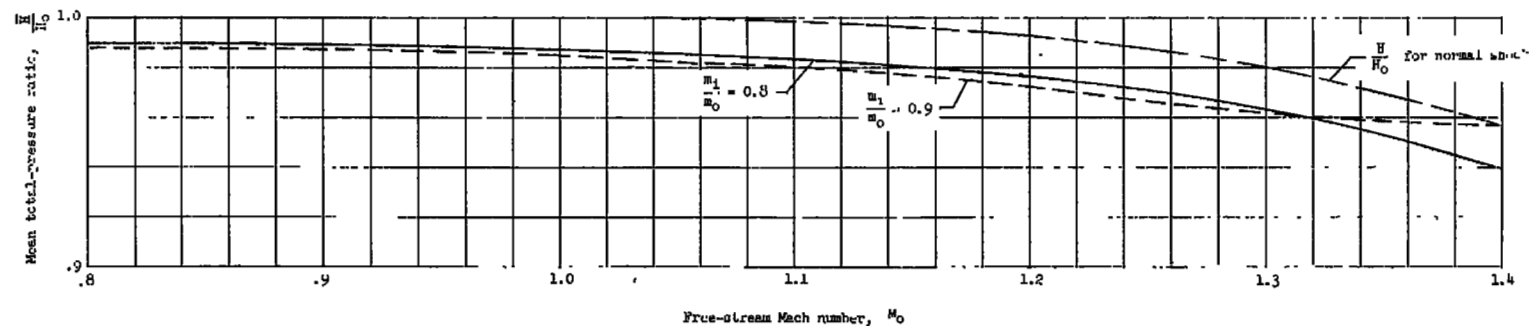


Figure 9.- Variation of mean total-pressure ratio with Mach number for inlet mass-flow ratios of 0.8 and 0.9.

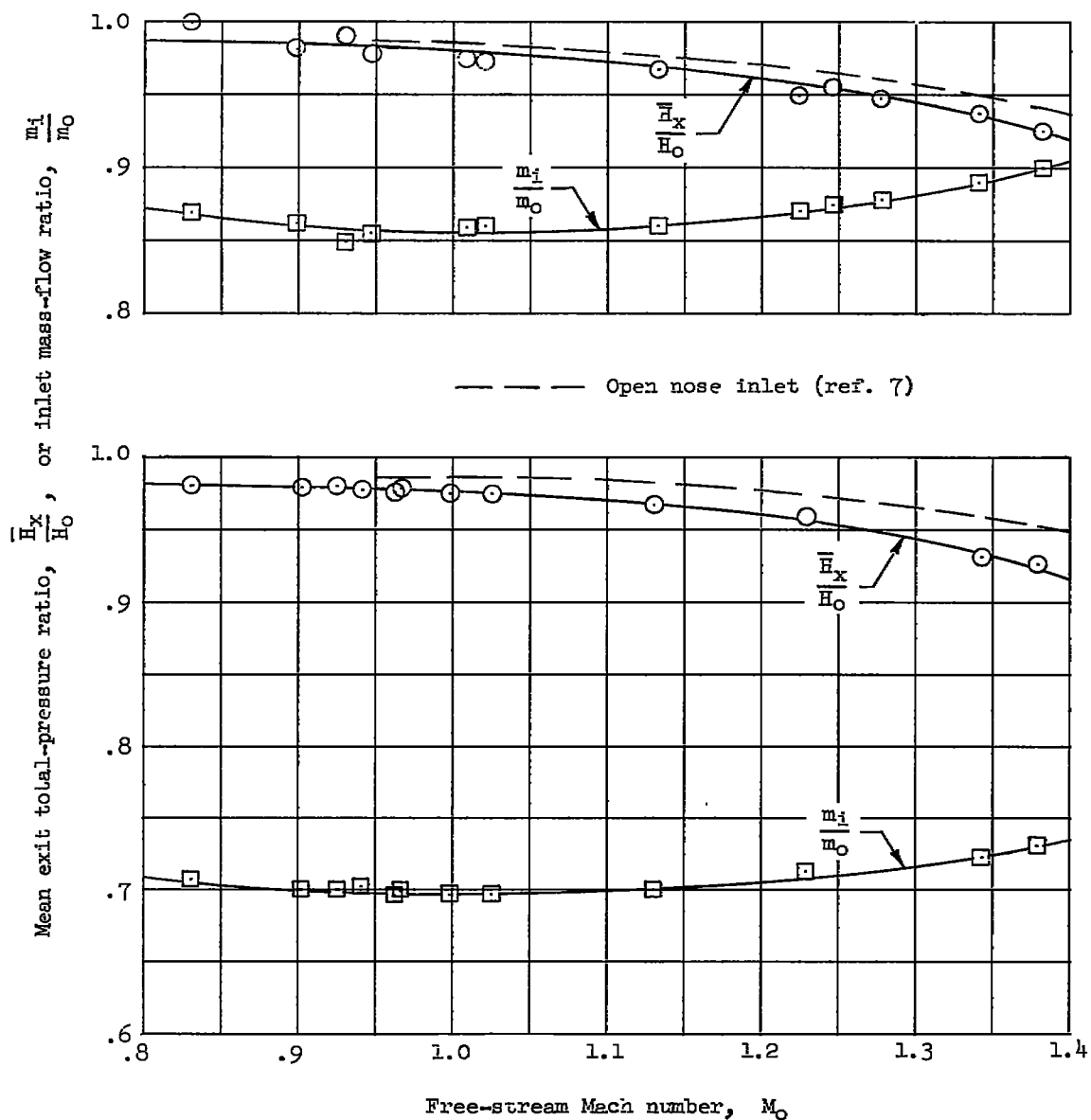


Figure 10.- The variation of mean total-pressure ratio and inlet mass-flow ratio with Mach number as obtained at the exit measuring station for two exit areas. (Inlet rake removed.)



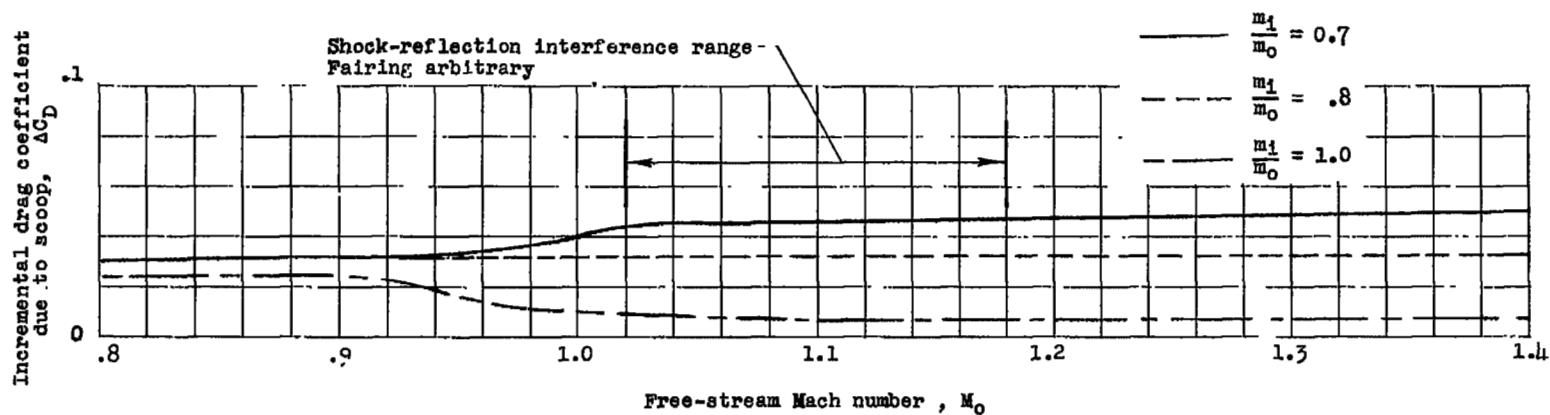


Figure 11.- The variation with Mach number of the drag increment due to the scoop for various inlet mass-flow ratios.

NASA Technical Library



3 1176 01438 0464

↑  
↓